

Runge–Kutta discontinuous Galerkin method using WENO limiters II: Unstructured meshes

Jun Zhu^{a,b}, Jianxian Qiu^{a,*}, Chi-Wang Shu^c, Michael Dumbser^d

^a Department of Mathematics, Nanjing University, Nanjing, Jiangsu 210093, PR China

^b College of Science, Nanjing University of Aeronautics and Astronautics, Nanjing, Jiangsu 210016, PR China

^c Division of Applied Mathematics, Brown University, Providence, RI 02912, USA

^d University of Trento, DICA Laboratory of Applied Mathematics, Via Mesiano, 77 I-38050 Trento, Italy

Received 25 September 2007; accepted 30 December 2007

Available online 11 January 2008

Abstract

In [J. Qiu, C.-W. Shu, Runge–Kutta discontinuous Galerkin method using WENO limiters, *SIAM Journal on Scientific Computing* 26 (2005) 907–929], Qiu and Shu investigated using weighted essentially non-oscillatory (WENO) finite volume methodology as limiters for the Runge–Kutta discontinuous Galerkin (RKDG) methods for solving nonlinear hyperbolic conservation law systems on structured meshes. In this continuation paper, we extend the method to solve two-dimensional problems on unstructured meshes, with the goal of obtaining a robust and high order limiting procedure to simultaneously obtain uniform high order accuracy and sharp, nonoscillatory shock transition for RKDG methods. Numerical results are provided to illustrate the behavior of this procedure.

© 2008 Elsevier Inc. All rights reserved.

MSC: 65M60; 65M99; 35L65

Keywords: Runge–Kutta discontinuous Galerkin method; Limiters; WENO finite volume scheme; High order accuracy

1. Introduction

In [20], Qiu and Shu investigated using weighted essentially non-oscillatory (WENO) finite volume methodology [16,14,11,13] as limiters for the Runge–Kutta discontinuous Galerkin (RKDG) finite element methods [6,5,4,3,7,8], for solving nonlinear hyperbolic conservation laws on structured meshes, with the goal of obtaining a robust and high order limiting procedure to simultaneously achieve uniform high order accuracy and sharp, nonoscillatory shock transition for the RKDG methods. In this continuation paper, we extend the method to solve two-dimensional nonlinear hyperbolic conservation laws:

* Corresponding author. Tel.: +86 25 8359 6053; fax: +86 25 8359 7130.

E-mail addresses: zhujun@nuaa.edu.cn (J. Zhu), jxqiu@nju.edu.cn (J. Qiu), shu@dam.brown.edu (C.-W. Shu), michael.dumbser@iag.uni-stuttgart.de (M. Dumbser).

$$\begin{cases} u_t + f(u)_x + g(u)_y = 0 \\ u(x, y, 0) = u_0(x, y) \end{cases} \quad (1.1)$$

on two-dimensional unstructured meshes.

WENO schemes have been designed in recent years as a class of high order finite volume or finite difference schemes to solve hyperbolic conservation laws with the property of maintaining both uniform high order accuracy and an essentially non-oscillatory shock transition. We have the third order finite volume WENO schemes in one space dimension in [16], the third and fifth order finite difference WENO schemes in multi-space dimensions with a general framework for the design of the smoothness indicators and nonlinear weights in [14], and finite volume WENO schemes on unstructured and structured meshes in [11,13,23,15,18]. WENO schemes are designed based on the successful ENO schemes in [12,25,26]. Both ENO and WENO schemes use the idea of adaptive stencils in the reconstruction procedure based on the local smoothness of the numerical solution to automatically achieve high order accuracy and a non-oscillatory property near discontinuities.

The first discontinuous Galerkin (DG) method was introduced in 1973 by Reed and Hill [22], in the framework of neutron transport (steady state linear hyperbolic equations). A major development of the DG method was carried out by Cockburn et al. in a series of papers [6,5,4,3,7], in which they established a framework to easily solve *nonlinear* time dependent hyperbolic conservation laws (1.1), using explicit, nonlinearly stable high order Runge–Kutta time discretizations [25] and DG discretization in space with exact or approximate Riemann solvers as interface fluxes and total variation bounded (TVB) limiter [24] to achieve non-oscillatory properties for strong shocks. These schemes are termed RKDG methods.

An important component of RKDG methods for solving the conservation laws (1.1) with strong shocks in the solutions is a nonlinear limiter, which is applied to detect discontinuities and control spurious oscillations near such discontinuities. Many such limiters have been used in the literature on RKDG methods. For example, we mention the *minmod* type TVB limiter [6,5,4,3,7], which is a slope limiter using a technique borrowed from the finite volume methodology; the moment based limiter [1] and an improved moment limiter [2], which are specifically designed for discontinuous Galerkin methods and work on the moments of the numerical solution. These limiters tend to degrade accuracy when mistakenly used in smooth regions of the solution.

In [20], Qiu and Shu initiated a study of using the WENO methodology as limiters for RKDG methods on structured mesh. The following framework has been adopted:

- Step 1. First, identify the “troubled cells”, namely those cells which might need the limiting procedure.
- Step 2. Then, replace the solution polynomials in those troubled cells by reconstructed polynomials using the WENO methodology which maintain the original cell averages (conservation), have the same orders of accuracy as before, but are less oscillatory.

This technique works quite well in our one and two-dimensional test problems in [20] and in the followup work [19,21] where the more compact Hermite WENO methodology was used in the troubled cells. More recently, Luo et al. [17], following [19,21], developed a Hermite WENO-based limiter for the second order RKDG method on unstructured meshes.

In this continuation paper, we extend the method to solve two dimensional problems on unstructured meshes. We use the usual WENO reconstruction based on the cell averages of neighboring cells to reconstruct the moments directly. This turns out to be a robust way to retain the original high order accuracy of the DG method. We describe the details of this procedure for the second and third order DG methods in Section 2 and present extensive numerical results in Section 3 to verify the accuracy and stability of this approach. Concluding remarks are given in Section 4.

2. WENO reconstruction as a limiter to the RKDG method on unstructured meshes

In this section we give the details of the procedure using the WENO reconstruction as a limiter for the RKDG method.

Given a triangulation consisting of cells Δ_j , $\mathbb{P}^k(\Delta_j)$ denotes the set of polynomials of degree at most k defined on Δ_j . Here k could actually change from cell to cell, but for simplicity we assume it is a constant over the whole triangulation. In the DG method, the solution as well as the test function space is given by $V_h^k = \{v(x, y) : v(x, y)|_{\Delta_j} \in \mathbb{P}^k(\Delta_j)\}$. We emphasize that the procedure described below does not depend on the specific basis chosen for the polynomials. We adopt a local orthogonal basis over a target cell, such as Δ_0 : $\{v_l^{(0)}(x, y), l = 0, \dots, K; K = (k + 1)(k + 2)/2 - 1\}$:

$$\begin{aligned} v_0^{(0)}(x, y) &= 1, \\ v_1^{(0)}(x, y) &= \frac{x - x_0}{\sqrt{|\Delta_0|}}, \\ v_2^{(0)}(x, y) &= a_{21} \frac{x - x_0}{\sqrt{|\Delta_0|}} + \frac{y - y_0}{\sqrt{|\Delta_0|}} + a_{22}, \\ v_3^{(0)}(x, y) &= \frac{(x - x_0)^2}{|\Delta_0|} + a_{31} \frac{x - x_0}{\sqrt{|\Delta_0|}} + a_{32} \frac{y - y_0}{\sqrt{|\Delta_0|}} + a_{33}, \\ v_4^{(0)}(x, y) &= a_{41} \frac{(x - x_0)^2}{|\Delta_0|} + \frac{(x - x_0)(y - y_0)}{|\Delta_0|} + a_{42} \frac{x - x_0}{\sqrt{|\Delta_0|}} + a_{43} \frac{y - y_0}{\sqrt{|\Delta_0|}} + a_{44}, \\ v_5^{(0)}(x, y) &= a_{51} \frac{(x - x_0)^2}{|\Delta_0|} + a_{52} \frac{(x - x_0)(y - y_0)}{|\Delta_0|} + \frac{(y - y_0)^2}{|\Delta_0|} + a_{53} \frac{x - x_0}{\sqrt{|\Delta_0|}} + a_{54} \frac{y - y_0}{\sqrt{|\Delta_0|}} + a_{55}, \dots \end{aligned}$$

where (x_0, y_0) and $|\Delta_0|$ are the barycenter and the area of the target cell Δ_0 , respectively. Then we would need to solve a linear system to obtain the values of a_{lm} by the orthogonality property:

$$\int_{\Delta_0} v_i^{(0)}(x, y)v_j^{(0)}(x, y) \, dx \, dy = w_i \delta_{ij} \tag{2.1}$$

with $w_i = \int_{\Delta_0} (v_i^{(0)}(x, y))^2 \, dx \, dy$.

The numerical solution $u^h(x, y, t)$ in the space V_h^k can be written as:

$$u^h(x, y, t) = \sum_{l=0}^K u_0^{(l)}(t)v_l^{(0)}(x, y) \quad \text{for } (x, y) \in \Delta_0$$

and the degrees of freedom $u_0^{(l)}(t)$ are the moments defined by

$$u_0^{(l)}(t) = \frac{1}{w_l} \int_{\Delta_0} u^h(x, y, t)v_l^{(0)}(x, y) \, dx \, dy, \quad l = 0, \dots, K.$$

In order to determine the approximate solution, we evolve the degrees of freedom $u_0^{(l)}(t)$:

$$\begin{aligned} \frac{d}{dt} u_0^{(l)}(t) &= \frac{1}{w_l} \left(\int_{\Delta_0} \left(f(u^h(x, y, t)) \frac{\partial}{\partial x} v_l^{(0)}(x, y) + g(u^h(x, y, t)) \frac{\partial}{\partial y} v_l^{(0)}(x, y) \right) dx \, dy \right. \\ &\quad \left. - \int_{\partial \Delta_0} (f(u^h(x, y, t)), g(u^h(x, y, t)))^T \cdot n v_l^{(0)}(x, y) \, ds \right), \quad l = 0, \dots, K. \end{aligned} \tag{2.2}$$

where n is the outward unit normal of the triangle boundary $\partial \Delta_0$.

In (2.2) the integral terms can be computed either exactly or by suitable numerical quadratures which are exact for polynomials of degree up to $2k$ for the element integral and up to $2k + 1$ for the edge integral. In this paper, we use A_G Gaussian points ($A_G = 6$ for $k = 1$ and $A_G = 7$ for $k = 2$) for the element quadrature and E_G Gaussian points ($E_G = 2$ for $k = 1$ and $E_G = 3$ for $k = 2$) for the edge quadrature:

$$\int_{\mathcal{A}_0} \left(f(u^h(x, y, t)) \frac{\partial}{\partial x} v_i^{(0)}(x, y) + g(u^h(x, y, t)) \frac{\partial}{\partial y} v_i^{(0)}(x, y) \right) dx dy \approx |\mathcal{A}_0| \sum_G \sigma_G \left(f(u^h(x_G, y_G, t)) \frac{\partial}{\partial x} v_i^{(0)}(x_G, y_G) + g(u^h(x_G, y_G, t)) \frac{\partial}{\partial y} v_i^{(0)}(x_G, y_G) \right) \tag{2.3}$$

$$\int_{\partial \mathcal{A}_0} (f(u^h(x, y, t)), g(u^h(x, y, t)))^T \cdot n v_i^{(0)}(x, y) ds \approx |\partial \mathcal{A}_0| \sum_G \bar{\sigma}_G (f(u^h(\bar{x}_G, \bar{y}_G, t)), g(u^h(\bar{x}_G, \bar{y}_G, t)))^T \cdot n v_i^{(0)}(\bar{x}_G, \bar{y}_G) \tag{2.4}$$

where $(x_G, y_G) \in \mathcal{A}_0$ and $(\bar{x}_G, \bar{y}_G) \in \partial \mathcal{A}_0$ are the Gaussian quadrature points, and σ_G and $\bar{\sigma}_G$ are the Gaussian quadrature weights. Since the edge integral is on element boundaries where the numerical solution is discontinuous, the flux $(f(u^h(x, y, t)), g(u^h(x, y, t)))^T \cdot n$ is replaced by a monotone numerical flux. The simple Lax–Friedrichs flux is used in all of our numerical tests. The semi-discrete scheme (2.2) is discretized in time by a non-linear stable Runge–Kutta time discretization, e.g. the third-order version

$$\begin{aligned} u^{(1)} &= u^n + \Delta t L(u^n), \\ u^{(2)} &= \frac{3}{4} u^n + \frac{1}{4} u^{(1)} + \frac{1}{4} \Delta t L(u^{(1)}), \\ u^{n+1} &= \frac{1}{3} u^n + \frac{2}{3} u^{(2)} + \frac{2}{3} \Delta t L(u^{(2)}). \end{aligned} \tag{2.5}$$

The method described above can compute solutions to (1.1), which are either smooth or have weak shocks and other discontinuities, without further modification. If the discontinuities are strong, however, the scheme will generate significant oscillations and even nonlinear instability. To avoid such difficulties, we borrow the technique of a slope limiter from the finite volume methodology and use it after each Runge–Kutta inner stage (or after the complete Runge–Kutta time step) to control the numerical solution.

In this paper, we will use the limiter adopted in [7] only to detect “troubled cells”. The main procedure is as follows. We use (x_{m_ℓ}, y_{m_ℓ}) , $\ell = 1, 2, 3$, to denote the midpoints of the edges on the boundary of the target cell \mathcal{A}_0 , and (x_{b_i}, y_{b_i}) , $i = 1, 2, 3$, to denote the barycenters of the neighboring triangles \mathcal{A}_i , $i = 1, 2, 3$, as shown in Fig. 2.1.

We then have

$$x_{m_1} - x_{b_0} = \alpha_1(x_{b_1} - x_{b_0}) + \alpha_2(x_{b_3} - x_{b_0}), \quad y_{m_1} - y_{b_0} = \alpha_1(y_{b_1} - y_{b_0}) + \alpha_2(y_{b_3} - y_{b_0}) \tag{2.6}$$

with nonnegative α_1, α_2 , which depend only on (x_{m_1}, y_{m_1}) and the geometry. We then define

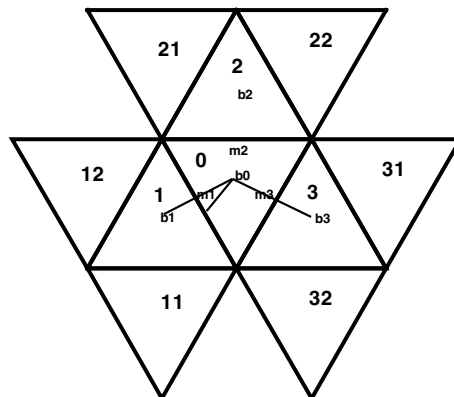


Fig. 2.1. The limiting diagram.

$$\tilde{u}^h(x_{m_1}, y_{m_1}, t) \equiv u^h(x_{m_1}, y_{m_1}, t) - u_0^{(0)}(t) \tag{2.7}$$

$$\Delta u(x_{m_1}, y_{m_1}, t) \equiv \alpha_1(u_1^{(0)}(t) - u_0^{(0)}(t)) + \alpha_2(u_3^{(0)}(t) - u_0^{(0)}(t)) \tag{2.8}$$

Using the TVB modified *minmod* function [24] defined as

$$\tilde{m}(a_1, a_2) = \begin{cases} a_1 & \text{if } |a_1| \leq M|a_0| \\ s \min(|a_1|, |a_2|) & \text{if } s = \text{sign}(a_1) = \text{sign}(a_2) \\ 0 & \text{otherwise} \end{cases} \tag{2.9}$$

where $M > 0$ is the TVB constant whose choice is problem dependent, we can compute the quantity

$$\tilde{u}^{\text{mod}} = \tilde{m}(\tilde{u}^h(x_{m_1}, y_{m_1}, t), \gamma \Delta u(x_{m_1}, y_{m_1}, t)) \tag{2.10}$$

with $\gamma > 1$ (we take $\gamma = 1.5$ in our numerical tests). If $\tilde{u}^{\text{mod}} \neq \tilde{u}^h(x_{m_1}, y_{m_1}, t)$, Δ_0 is marked as a “troubled cell” for further reconstruction. This procedure is repeated for the other two edges of Δ_0 as well. Since the WENO reconstruction maintains high order accuracy in the troubled cells, it is less crucial to choose an accurate M . We present in Section 3 numerical tests obtained with different choices of M .

For the troubled cells, we reconstruct the polynomial solutions while retaining their cell averages. In other words, we reconstruct the degrees of freedom $u_0^{(l)}(t)$, $l = 1, \dots, K$ and retain only the cell average $u_0^{(0)}(t)$.

For the $k = 1$ case, we summarize the procedure to reconstruct the first order moments $u_0^{(1)}(t)$ and $u_0^{(2)}(t)$ in the troubled cell Δ_0 using the WENO reconstruction procedure. For simplicity, we relabel the “troubled cell” and its neighboring cells as shown in Fig. 2.2.

- Step 1. We select the big stencil as $S = \{\Delta_0, \Delta_1, \Delta_2, \Delta_3, \Delta_{11}, \Delta_{12}, \Delta_{21}, \Delta_{22}, \Delta_{31}, \Delta_{32}\}$. Then we construct a quadratic polynomial $P(x, y)$ to obtain a third order approximation of u by requiring that it has the same cell average as u on the target cell Δ_0 , and matches the cell averages of u on the other triangles in the set $S \setminus \{\Delta_0\}$ in a least-square sense, see [13].
- Step 2. We divide S into nine smaller stencils:

$$\begin{aligned} S_1 &= \{\Delta_0, \Delta_1, \Delta_2\}, & S_2 &= \{\Delta_0, \Delta_2, \Delta_3\}, & S_3 &= \{\Delta_0, \Delta_3, \Delta_1\}, & S_4 &= \{\Delta_0, \Delta_1, \Delta_{11}\}, \\ S_5 &= \{\Delta_0, \Delta_1, \Delta_{12}\}, & S_6 &= \{\Delta_0, \Delta_2, \Delta_{21}\}, & S_7 &= \{\Delta_0, \Delta_2, \Delta_{22}\}, \\ S_8 &= \{\Delta_0, \Delta_3, \Delta_{31}\}, & S_9 &= \{\Delta_0, \Delta_3, \Delta_{32}\}. \end{aligned}$$

We then construct nine linear polynomials $q_i(x, y)$, $i = 1, \dots, 9$, satisfying

$$\frac{1}{|\Delta_\ell|} \int_{\Delta_\ell} q_i(x, y) \, dx \, dy = \bar{u}_\ell, \quad \text{for } \Delta_\ell \in S_i. \tag{2.11}$$

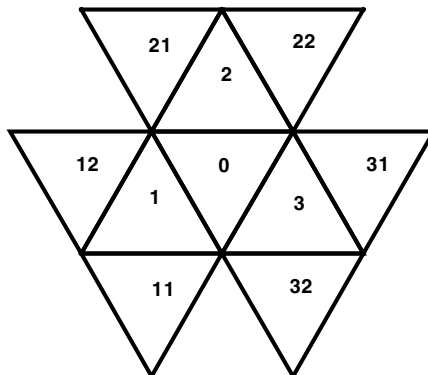


Fig. 2.2. The big stencil S .

Step 3. We find the combination coefficients, also called linear weights, denoted by $\gamma_1^{(l)}, \dots, \gamma_9^{(l)}$, $l = 1, 2$, satisfying

$$\int_{\Delta_0} P(x, y) v_l^{(0)}(x, y) dx dy = \sum_{i=1}^9 \gamma_i^{(l)} \int_{\Delta_0} q_i(x, y) v_l^{(0)}(x, y) dx dy, \quad l = 1, 2 \tag{2.12}$$

for the quadratic polynomial $P(x, y)$ defined before. The linear weights are achieved by asking for

$$\min \left(\sum_{i=1}^9 (\gamma_i^{(l)})^2 \right), \quad l = 1, 2. \tag{2.13}$$

By doing so, we can get the linear weights uniquely but can not guarantee their positivity. We use the method introduced in [13,23] to overcome this difficulty.

Step 4. We compute the smoothness indicators, denote by β_i , $i = 1, \dots, 9$, for the smaller stencils S_i , $i = 1, \dots, 9$, which measure how smooth the functions $q_i(x, y)$, $i = 1, \dots, 9$ are in the target cell Δ_0 . The smaller these smoothness indicators, the smoother the functions are in the target cell. We use the same recipe for the smoothness indicators as in [14]:

$$\beta_i = \sum_{|\ell|=1}^k |\Delta_0|^{|\ell|-1} \int_{\Delta_0} \left(\frac{\partial^{|\ell|}}{\partial x^{\ell_1} \partial y^{\ell_2}} q_i(x, y) \right)^2 dx dy \tag{2.14}$$

where $\ell = (\ell_1, \ell_2)$.

Step 5. We compute the non-linear weights based on the smoothness indicators:

$$\omega_i = \frac{\bar{\omega}_i}{\sum_{\ell=1}^9 \bar{\omega}_\ell}, \quad \bar{\omega}_\ell = \frac{\gamma_\ell}{(\varepsilon + \beta_\ell)^2}. \tag{2.15}$$

Here ε is a small positive number to avoid the denominator to become zero. We take $\varepsilon = 10^{-6}$ in our computation.

The moments of the reconstructed polynomial are then given by:

$$u_0^{(l)}(t) = \frac{1}{\int_{\Delta_0} (v_l^{(0)}(x, y))^2 dx dy} \sum_{i=1}^9 \omega_i^{(l)} \int_{\Delta_0} q_i(x, y) v_l^{(0)}(x, y) dx dy, \quad l = 1, 2. \tag{2.16}$$

For the $k = 2$ case, the procedure to reconstruct the first and second order moments $u_0^{(1)}(t)$, $u_0^{(2)}(t)$, $u_0^{(3)}(t)$, $u_0^{(4)}(t)$ and $u_0^{(5)}(t)$ in the troubled cell Δ_0 is analogous to that for the $k = 1$ case. The troubled cell and its neighboring cells are shown in Fig. 2.3.

Step 1. We select the big stencil as $T = \{\Delta_0, \Delta_1, \Delta_2, \Delta_3, \Delta_{11}, \Delta_{12}, \Delta_{21}, \Delta_{22}, \Delta_{31}, \Delta_{32}, \Delta_{112}, \Delta_{121}, \Delta_{212}, \Delta_{221}, \Delta_{312}, \Delta_{321}\}$. Then we construct a fourth degree polynomial $Q(x, y)$ to obtain a fifth order approximation of u by requiring that it has the same cell average as u on the target cell Δ_0 and matches the cell averages of u on the other triangles in the set $T \setminus \{\Delta_0\}$ in a least-square sense.

Step 2. We divide T into nine smaller stencils:

$$\begin{aligned} T_1 &= \{\Delta_0, \Delta_1, \Delta_{11}, \Delta_{12}, \Delta_3, \Delta_{32}\}, & T_2 &= \{\Delta_0, \Delta_1, \Delta_{11}, \Delta_{12}, \Delta_2, \Delta_{21}\}, & T_3 &= \{\Delta_0, \Delta_2, \Delta_{21}, \Delta_{22}, \Delta_1, \Delta_{12}\}, \\ T_4 &= \{\Delta_0, \Delta_2, \Delta_{21}, \Delta_{22}, \Delta_3, \Delta_{31}\}, & T_5 &= \{\Delta_0, \Delta_3, \Delta_{31}, \Delta_{32}, \Delta_2, \Delta_{22}\}, & T_6 &= \{\Delta_0, \Delta_3, \Delta_{31}, \Delta_{32}, \Delta_1, \Delta_{11}\}, \\ T_7 &= \{\Delta_0, \Delta_1, \Delta_{11}, \Delta_{12}, \Delta_{112}, \Delta_{121}\}, & T_8 &= \{\Delta_0, \Delta_2, \Delta_{21}, \Delta_{22}, \Delta_{212}, \Delta_{221}\}, \\ T_9 &= \{\Delta_0, \Delta_3, \Delta_{31}, \Delta_{32}, \Delta_{312}, \Delta_{321}\}. \end{aligned}$$

We can then construct quadratic polynomials $q_i(x, y)$, $i = 1, \dots, 9$, which satisfy the following conditions

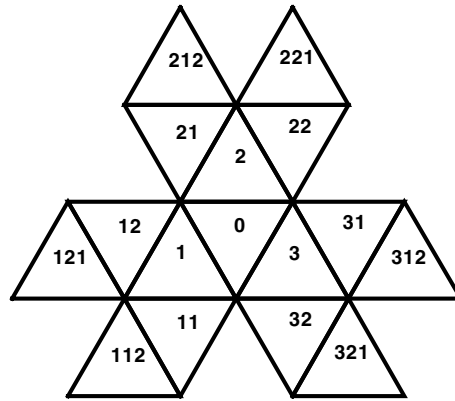


Fig. 2.3. The big stencil T .

$$\frac{1}{|\Delta_\ell|} \int_{\Delta_\ell} q_i(x, y) \, dx \, dy = \bar{u}_\ell, \quad \text{for } \Delta_\ell \in T_i. \tag{2.17}$$

The remaining steps 3, 4 and 5 are the same as those for the $k = 1$ case. Finally, the moments of the reconstructed polynomial are given by

$$u_0^{(l)}(t) = \frac{1}{\int_{\Delta_0} (v_i^{(0)}(x, y))^2 \, dx \, dy} \sum_{i=1}^9 \omega_i^{(l)} \int_{\Delta_0} q_i(x, y) v_i^{(0)}(x, y) \, dx \, dy, \quad l = 1, 2, 3, 4, 5. \tag{2.18}$$

3. Numerical results

In this section we provide numerical results to demonstrate the performance of the WENO reconstruction limiters for the RKDG methods on unstructured meshes described in Section 2.

We first test the accuracy of the schemes in two-dimensional problems.

Example 3.1. We solve the following nonlinear scalar Burgers equation in two dimensions:

$$u_t + \left(\frac{u^2}{2}\right)_x + \left(\frac{u^2}{2}\right)_y = 0 \tag{3.1}$$

with the initial condition $u(x, y, 0) = 0.5 + \sin(\pi(x + y)/2)$ and periodic boundary conditions in both directions. We compute the solution up to $t = 0.5/\pi$, when the solution is still smooth. For this test case, the coarsest mesh we use is shown in Fig. 3.1. The errors and numerical orders of accuracy for the RKDG method with the WENO limiter comparing with the original RKDG method without limiter are shown in Table 3.1. In order to magnify the possible effect of the WENO limiter on accuracy, we have deliberately chosen a small TVB constant $M = 0.01$ so that many cells are identified as “troubled cells”. We can see that the WENO limiter keeps the designed order of accuracy, however the magnitude of the errors is larger than that of the original RKDG method on the same mesh.

Example 3.2. We solve the Euler equations

$$\frac{\partial}{\partial t} \begin{pmatrix} \rho \\ \rho u \\ \rho v \\ E \end{pmatrix} + \frac{\partial}{\partial x} \begin{pmatrix} \rho u \\ \rho u^2 + p \\ \rho uv \\ u(E + p) \end{pmatrix} + \frac{\partial}{\partial y} \begin{pmatrix} \rho v \\ \rho uv \\ \rho v^2 + p \\ v(E + p) \end{pmatrix} = 0 \tag{3.2}$$

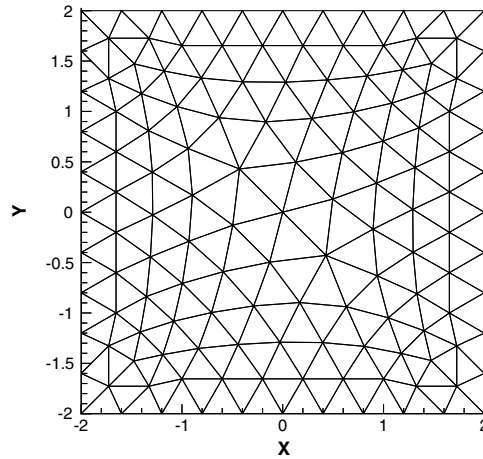


Fig. 3.1. Burgers equation. Mesh. Triangle: $h = 4/10$.

Table 3.1
 $u_t + \left(\frac{u^2}{2}\right)_x + \left(\frac{u^2}{2}\right)_y = 0, u(x, y, 0) = 0.5 + \sin(\pi(x + y)/2)$

	h	DG with WENO limiter				DG without limiter			
		L^1 error	Order	L^∞ error	Order	L^1 error	Order	L^∞ error	Order
P^1	4/10	5.11E-2		5.28E-1		2.41E-2		2.56E-1	
	4/20	1.31E-2	1.96	1.91E-1	1.46	6.07E-3	1.99	7.54E-2	1.77
	4/40	3.21E-3	2.02	5.05E-2	1.92	1.53E-3	1.98	2.14E-2	1.81
	4/80	7.80E-4	2.04	1.43E-2	1.81	3.91E-4	1.97	5.71E-3	1.91
	4/160	1.59E-4	2.29	3.61E-3	1.99	9.87E-5	1.99	1.55E-3	1.88
P^2	4/10	6.91E-3		1.40E-1		1.70E-3		5.28E-2	
	4/20	8.60E-4	3.01	2.31E-2	2.60	2.45E-4	2.79	8.19E-3	2.69
	4/40	1.05E-4	3.03	4.23E-3	2.45	3.17E-5	2.95	1.55E-3	2.39
	4/80	1.60E-5	2.71	6.81E-4	2.63	4.01E-6	2.98	2.37E-4	2.71
	4/160	2.10E-6	2.93	1.01E-4	2.75	5.03E-7	3.00	3.20E-5	2.89

Periodic boundary conditions in both directions. $t = 0.5/\pi$. L^1 and L^∞ errors. RKDG with the WENO limiter ($M = 0.01$) compared to RKDG without limiter. The mesh points on the boundary are uniformly distributed with cell length h .

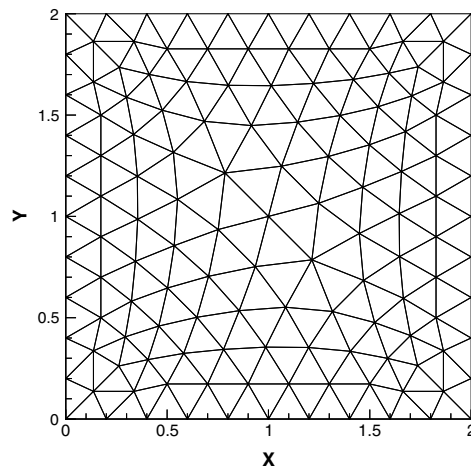


Fig. 3.2. 2D-Euler equations. Mesh. Triangle: $h = 2/10$.

Table 3.2

2D-Euler equations: initial data $\rho(x, y, 0) = 1 + 0.2 \sin(\pi(x + y))$, $u(x, y, 0) = 0.7$, $v(x, y, 0) = 0.3$, and $p(x, y, 0) = 1$

	h	DG with WENO limiter				DG without limiter			
		L^1 error	Order	L^∞ error	Order	L^1 error	Order	L^∞ error	Order
P^1	2/10	3.76E-2		8.37E-2		4.39E-3		2.23E-2	
	2/20	1.16E-2	1.69	3.50E-2	1.26	1.03E-3	2.08	5.42E-3	2.04
	2/40	2.36E-3	2.31	1.25E-2	1.48	2.54E-4	2.02	1.29E-3	2.06
	2/80	3.99E-4	2.56	3.83E-3	1.70	6.38E-5	1.99	3.27E-4	1.98
	2/160	7.33E-5	2.44	1.16E-3	1.72	1.62E-5	1.97	8.48E-5	1.95
P^2	2/10	4.01E-3		1.76E-2		4.48E-4		5.94E-3	
	2/20	6.50E-4	2.63	3.47E-3	2.34	6.17E-5	2.86	1.14E-3	2.38
	2/40	8.37E-5	2.96	4.94E-4	2.81	7.05E-6	3.12	1.94E-4	2.56
	2/80	1.01E-5	3.04	6.60E-5	2.91	7.76E-7	3.18	2.87E-5	2.76
	2/160	1.26E-6	3.01	7.09E-6	3.21	1.10E-7	2.81	3.62E-6	2.99

Periodic boundary conditions in both directions. $t = 2.0$. L^1 and L^∞ errors. RKDG with the WENO limiter ($M = 0.01$) compared to RKDG without limiter. The mesh points on the boundary are uniformly distributed with cell length h .

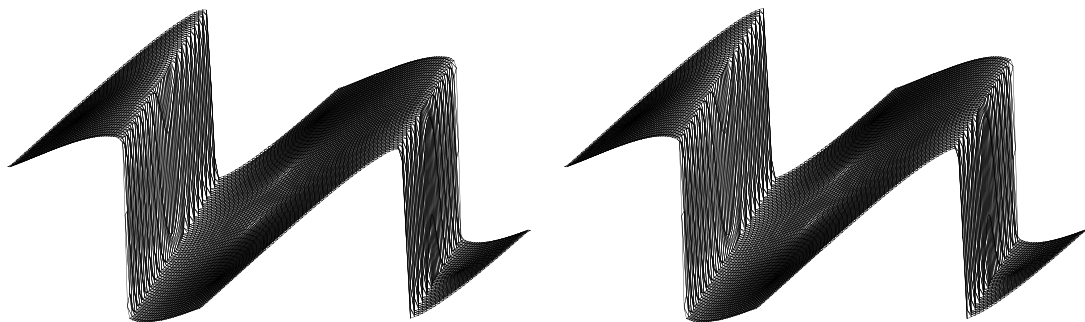


Fig. 3.3. Burgers equation. $t = 1.5/\pi$. The surface of the solution. Triangle: $h = 4/80$. RKDG with the WENO limiter, $M = 0.01$. Left: second order ($k = 1$); right: third order ($k = 2$).

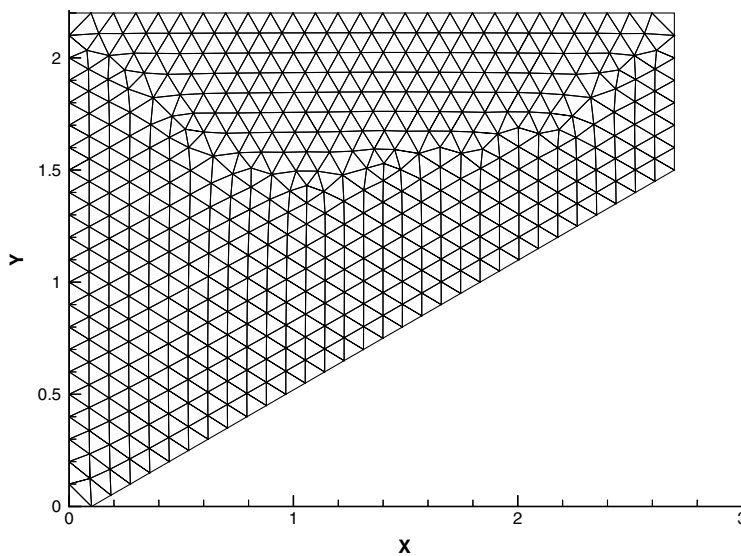


Fig. 3.4. Double Mach reflection problem. Sample mesh. The mesh points on the boundary are uniformly distributed with cell length $h = 1/10$.

in which ρ is the density, u is the x -direction velocity, v is the y -direction velocity, E is the total energy, and $p = (\gamma - 1)(E - \frac{1}{2}\rho(u^2 + v^2))$ is the pressure, with $\gamma = 1.4$. The initial conditions are: $\rho(x, y, 0) = 1 + 0.2 \sin(\pi(x + y))$, $u(x, y, 0) = 0.7$, $v(x, y, 0) = 0.3$, $p(x, y, 0) = 1$. Periodic boundary conditions are applied in both directions. The exact solution is $\rho(x, y, t) = 1 + 0.2 \sin(\pi(x + y - t))$. We compute the solution up to $t = 2$. For this test case, the coarsest mesh we use is shown in Fig. 3.2. The errors and numerical orders of accuracy of the density for the RKDG method with the WENO limiter comparing with the original RKDG method without a limiter are shown in Table 3.2. Similar to the previous example, we have again chosen a small TVB constant $M = 0.01$ so that many cells are identified as “troubled cells”. We can see that the WENO limiter again keeps the designed order of accuracy, with the magnitude of the errors larger than that of the original RKDG method on the same mesh.

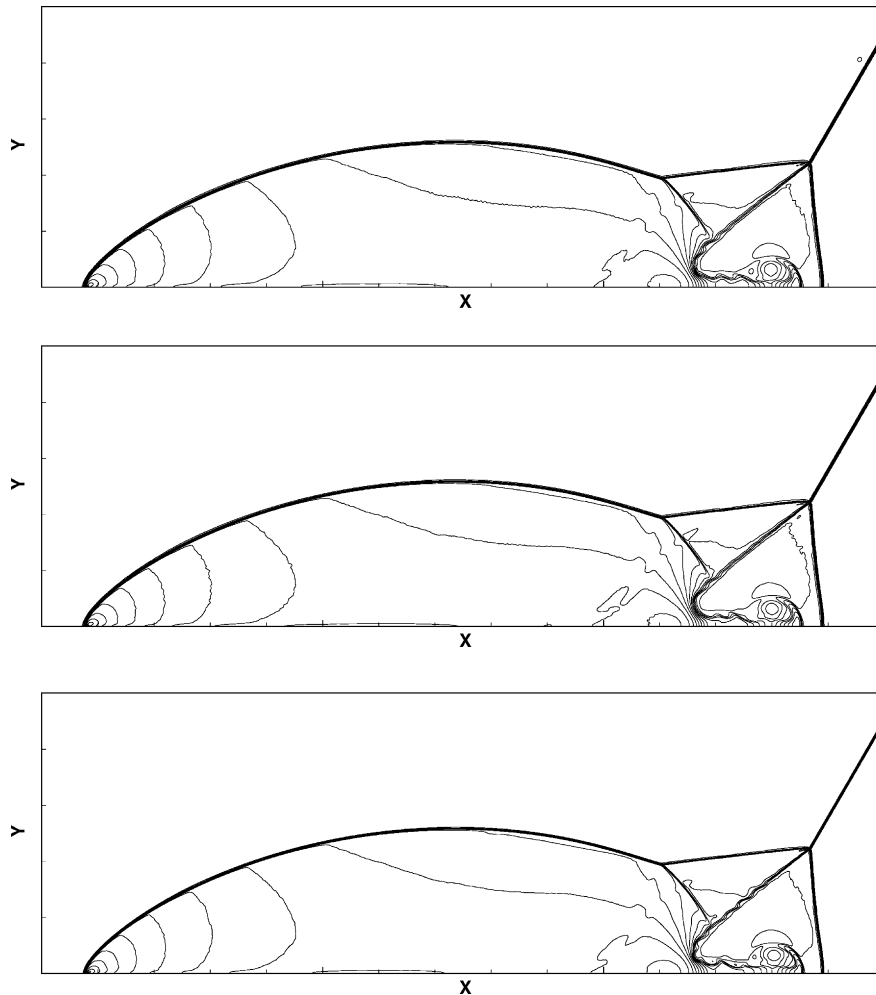


Fig. 3.5. Double Mach reflection problem. Second order ($k = 1$) RKDG with the WENO limiter. Thirty equally spaced density contours from 1.5 to 22.7. The mesh points on the boundary are uniformly distributed with cell length $h = 1/300$. Top: the TVB constant $M = 1$; middle: $M = 50$; bottom: $M = 100$.

We now test the performance of the RKDG method with the WENO limiters for problems containing shocks. For a direct comparison with the RKDG method using the original *minmod* TVB limiter, we refer to the results in [5,4,3,7]. In general, the results are comparable when M is chosen adequately. When M is chosen too small, however, the RKDG method with the WENO limiter produces much better results than those with the original *minmod* TVB limiter.

Example 3.3. We solve the same nonlinear Burgers equation (3.1) with the same initial condition $u(x, y, 0) = 0.5 + \sin(\pi(x + y)/2)$, except that we plot the results at $t = 1.5/\pi$ when a shock has already appeared in the solution. The solutions are shown in Fig. 3.3. We can see that the schemes give non-oscillatory shock transitions for this problem.

Example 3.4. Double Mach reflection problem. This model problem is originally from [27]. We solve the Euler equations (3.2) in a computational domain of a tube which contains a 30° wedge. The shock moves with a Mach number of 10, the undisturbed air ahead the shock has a density of 1.4 and a pressure of 1 and the left hand side of the shock has a density of 8, velocity of 8.25 and pressure of 116.5. The results are shown at

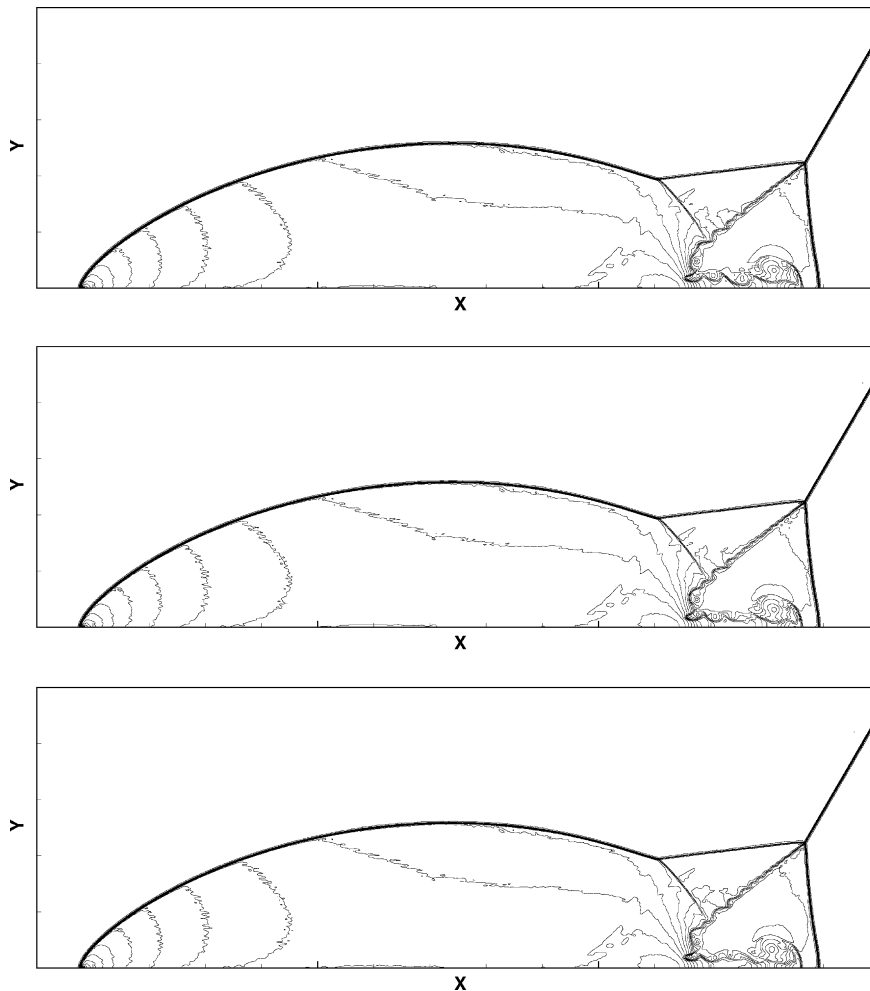


Fig. 3.6. Double Mach reflection problem. Third order ($k = 2$) RKDG with the WENO limiter. Thirty equally spaced density contours from 1.5 to 22.7. The mesh points on the boundary are uniformly distributed with cell length $h = 1/300$. Top: the TVB constant $M = 1$; middle: $M = 50$; bottom: $M = 100$.

$t = 0.2$. Two different orders of accuracy for the RKDG with WENO limiters, $k = 1$ and $k = 2$ (second and third order), as well as three different values of the TVB constant, $M = 1$, $M = 50$ and $M = 100$, are used in the numerical experiments. A sample mesh coarser than what is used in the actual computation is shown in Fig. 3.4. The simulation results on the mesh with different values of M are shown in Figs. 3.5 and 3.6. The

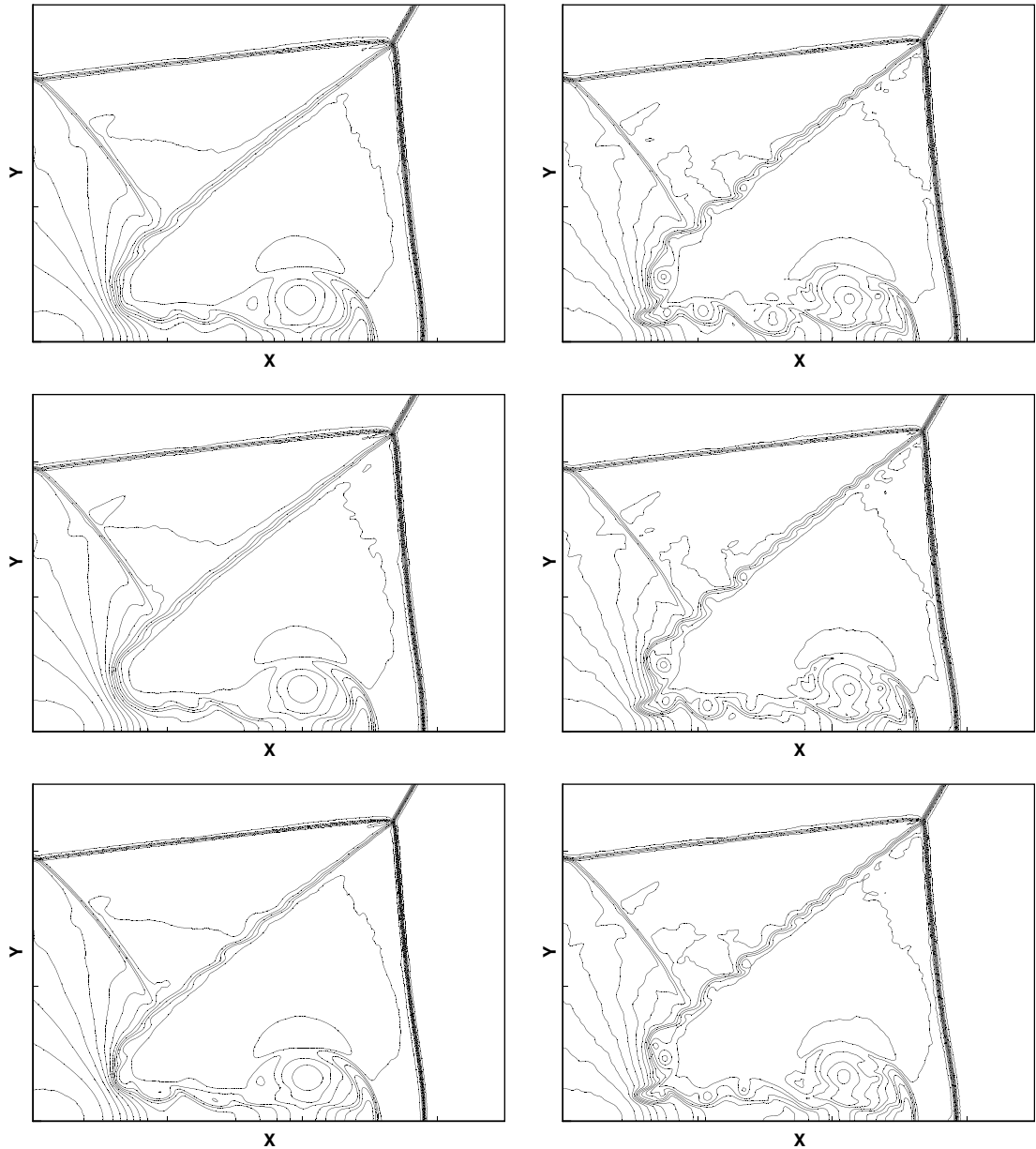


Fig. 3.7. Double Mach reflection problem. RKDG with WENO limiter. Zoom-in pictures around the Mach stem. Thirty equally spaced density contours from 1.5 to 22.7. Left: second order ($k = 1$); right: third order ($k = 2$). The mesh points on the boundary are uniformly distributed with cell length $h = 1/300$. Top: the TVB constant $M = 1$; middle: $M = 50$; bottom: $M = 100$.

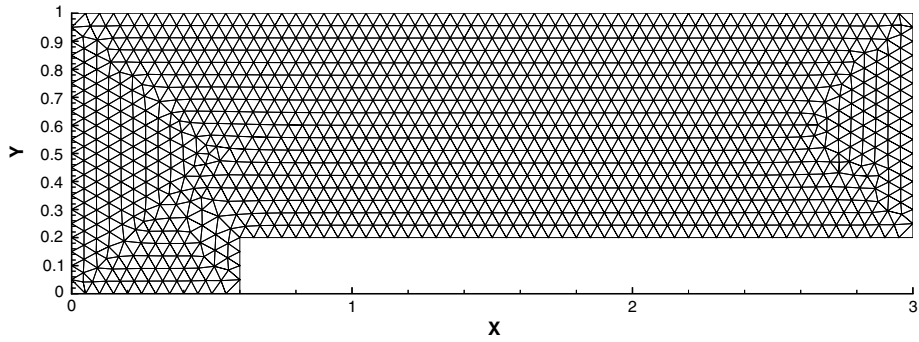


Fig. 3.8. Forward step problem. Sample mesh. The mesh points on the boundary are uniformly distributed with cell length $h = 1/20$.

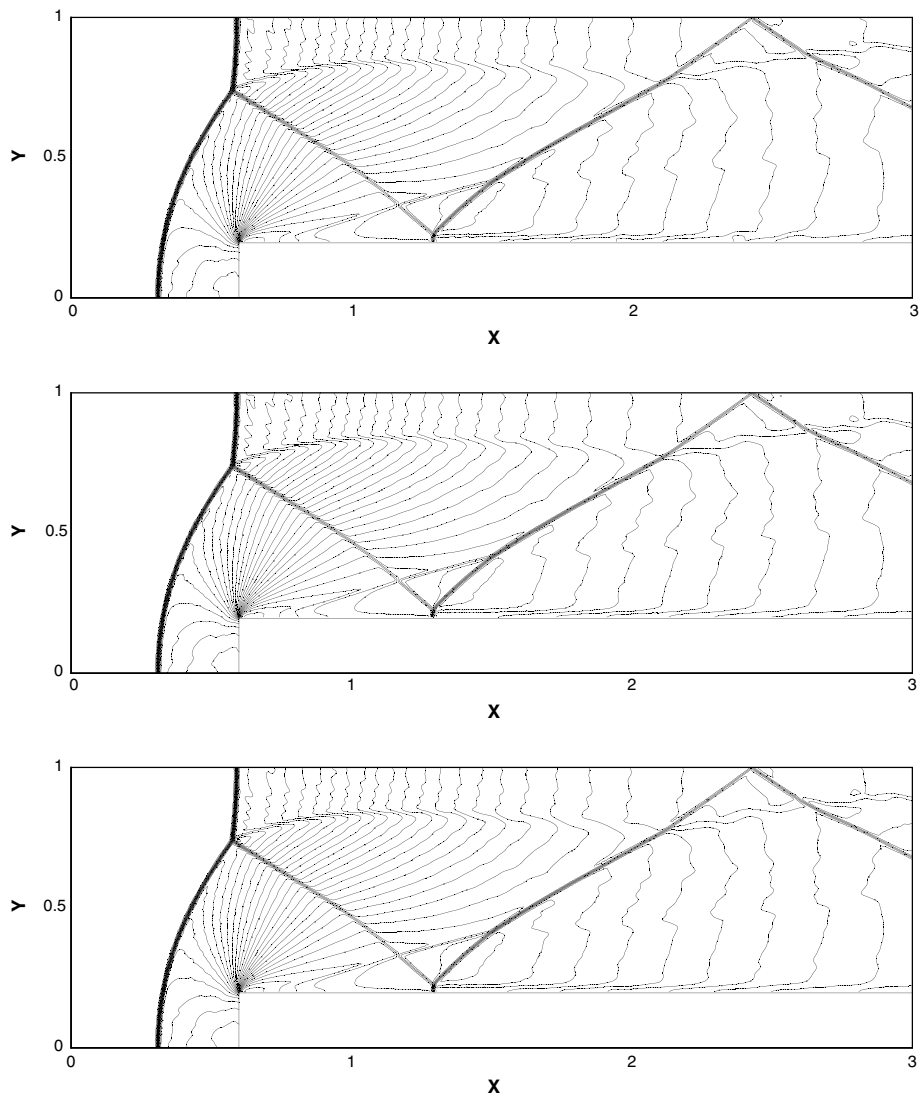


Fig. 3.9. Forward step problem. Second order ($k = 1$) RKDG with the WENO limiter. Thirty equally spaced density contours from 0.32 to 6.15. The mesh points on the boundary are uniformly distributed with cell length $h = 1/160$. Top: the TVB constant $M = 1$; middle: $M = 50$; bottom: $M = 100$.

“zoomed-in” pictures around the double Mach stem to show more details are given in Fig. 3.7. All the figures are showing 30 equally spaced density contours from 1.5 to 22.7. Clearly, the resolution improves with an increasing k on the same mesh. Also, the resolution is slightly better for $M = 100$ than for $M = 1$, however this difference is not significant.

Example 3.5. A Mach 3 wind tunnel with a step. This model problem is also originally from [27]. The setup of the problem is as follows. The wind tunnel is 1 length unit wide and 3 length units long. The step is 0.2 length units high and is located 0.6 length units from the left-hand end of the tunnel. The problem is initialized by a right-going Mach 3 flow. Reflective boundary conditions are applied along the wall of the tunnel and inflow/outflow boundary conditions are applied at the entrance/exit. At the corner of the step, there is a singularity. However we do not modify our schemes or refine the mesh near the corner, in order to test the performance of our schemes for such singularity. The results are shown at $t = 4$. We present a sample triangulation of the

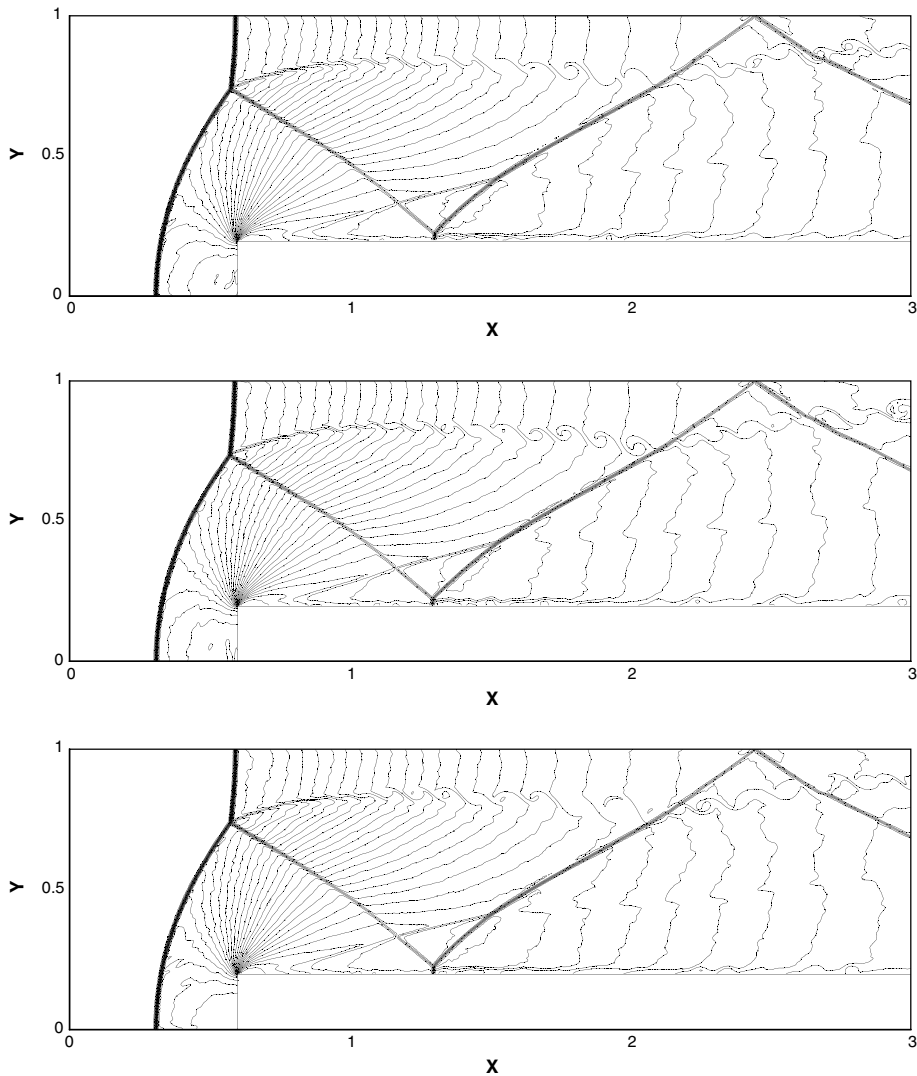


Fig. 3.10. Forward step problem. Third order ($k = 2$) RKDG with the WENO limiter. Thirty equally spaced density contours from 0.32 to 6.15. The mesh points on the boundary are uniformly distributed with cell length $h = 1/160$. Top: the TVB constant $M = 1$; middle: $M = 50$; bottom: $M = 100$.

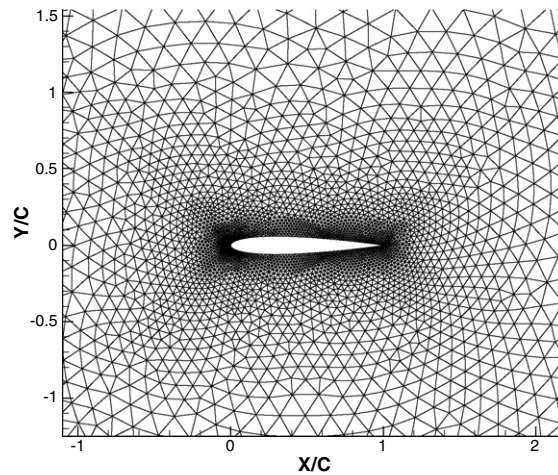


Fig. 3.11. NACA0012 airfoil mesh zoom in.

Table 3.3
NACA0012 airfoil problem

		$M_\infty = 0.8$, angle of attack $\alpha = 1.25^\circ$			$M_\infty = 0.85$, angle of attack $\alpha = 1^\circ$			
P^1	TVB constant M	1	10	100	TVB constant M	1	10	100
	Maximum percentage	30.0	20.4	9.83	Maximum percentage	30.9	21.9	11.1
	Average percentage	19.3	11.6	5.45	Average percentage	20.9	14.0	7.01
P^2	TVB constant M	1	10	100	TVB constant M	1	10	100
	Maximum percentage	52.1	43.2	17.9	Maximum percentage	52.8	43.8	19.0
	Average percentage	30.9	16.6	6.77	Average percentage	33.5	21.0	8.71

The maximum and average percentages of troubled cells subject to the WENO limiting.

whole region $[0, 3] \times [0, 1]$ in Fig. 3.8. In Figs. 3.9 and 3.10, we show 30 equally spaced density contours from 0.32 to 6.15 computed by the second and third order RKDG schemes with the WENO limiters, for the TVB constant $M = 1$, $M = 50$ and $M = 100$, respectively. We can clearly observe that the third order scheme gives better resolution than the second order scheme, especially for the resolution of the physical instability and roll-up of the contact line.

Example 3.6. We consider inviscid Euler transonic flow past a single NACA0012 airfoil configuration with Mach number $M_\infty = 0.8$, angle of attack $\alpha = 1.25^\circ$ and with $M_\infty = 0.85$, angle of attack $\alpha = 1^\circ$. The computational domain is $[-15, 15] \times [-15, 15]$. The mesh used in the computation is shown in Fig. 3.11, consisting of 9340 elements with the maximum diameter of the circumscribed circle being 1.4188 and the minimum diameter being 0.0031 near the airfoil. The mesh uses curved cells near the airfoil. The second order RKDG scheme with the WENO limiter and the TVB constant $M = 1$, $M = 10$ and $M = 100$, and the third order scheme with $M = 1$, $M = 10$ and $M = 100$, are used in the numerical experiments. In Table 3.3 we document the percentage of cells declared to be “troubled cells” for different orders of accuracy and different TVB constant M in the *minmod* limiter to identify troubled cells. We can see that only a small percentage of cells are declared as “troubled cells” for large M . Mach number and pressure distributions are shown in Figs. 3.12–3.14 and 3.15, respectively. We can see that the third order scheme has better resolution than the second order one. The troubled cells identified at the last time step are shown in Figs. 3.16 and 3.17. Clearly, fewer cells are identified as “troubled cells” for larger M . Finally, the reduction of density residual as a function of the number of iterations is shown in Figs. 3.18 and 3.19.

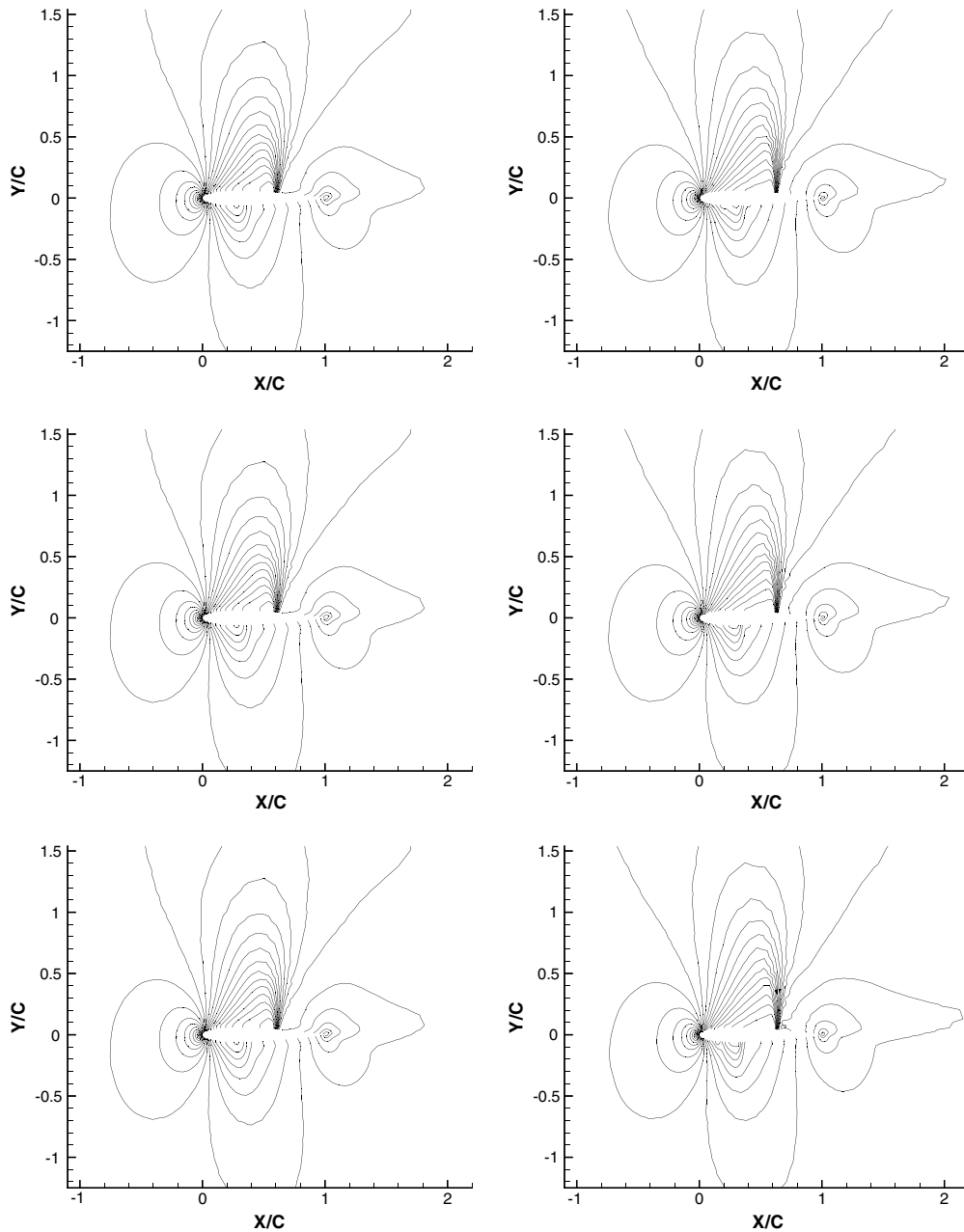


Fig. 3.12. NACA0012 airfoil. $M_\infty = 0.8$, angle of attack $\alpha = 1.25^\circ$. Mach number. RKDG with the WENO limiter. Thirty equally spaced Mach number contours from 0.172 to 1.325. Left: second order ($k = 1$); right: third order ($k = 2$). Top: the TVB constant $M = 1$; middle: $M = 10$; bottom: $M = 100$.

4. Concluding remarks

We have developed a limiter for the RKDG methods solving hyperbolic conservation laws using finite volume high order WENO reconstructions on unstructured meshes. The idea is to first identify troubled cells subject to the WENO limiting, using a TVB *minmod*-type limiter, then reconstruct the polynomial solution inside the troubled cells by the WENO reconstruction using the cell averages of neighboring cells, while maintaining

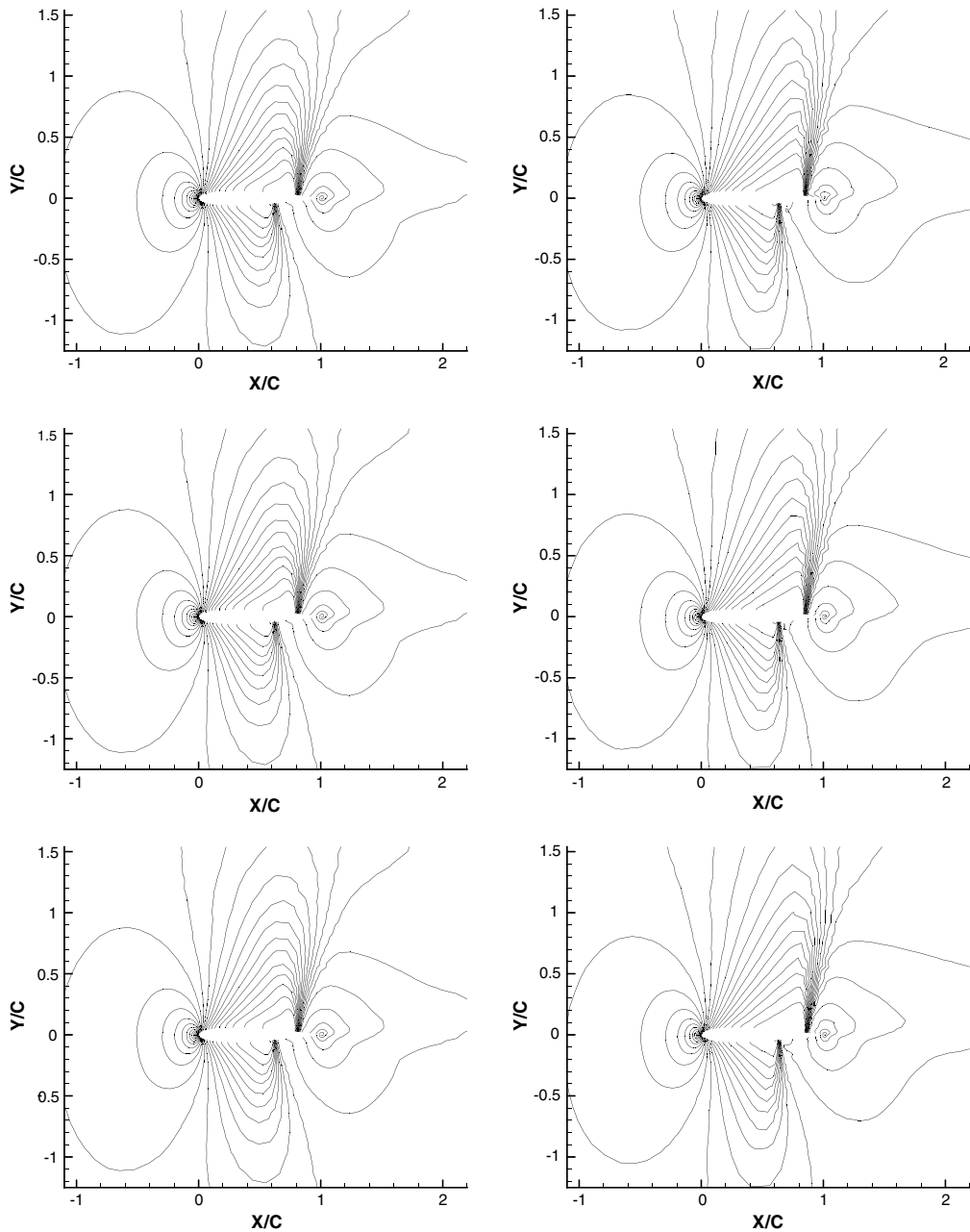


Fig. 3.13. NACA0012 airfoil. $M_\infty = 0.85$, angle of attack $\alpha = 1^\circ$. Mach number. RKDG with the WENO limiter. Thirty equally spaced Mach number contours from 0.158 to 1.357. Left: second order ($k = 1$); right: third order ($k = 2$). Top: the TVB constant $M = 1$; middle: $M = 10$; bottom: $M = 100$.

the original cell averages of the troubled cells. Numerical results are provided to show that the method is stable, accurate, and robust in maintaining accuracy. Further work will be carried out including even higher order WENO limiters on unstructured triangular meshes as well as an extension to three dimensional tetrahedral meshes using the WENO approaches in [9,10,28].

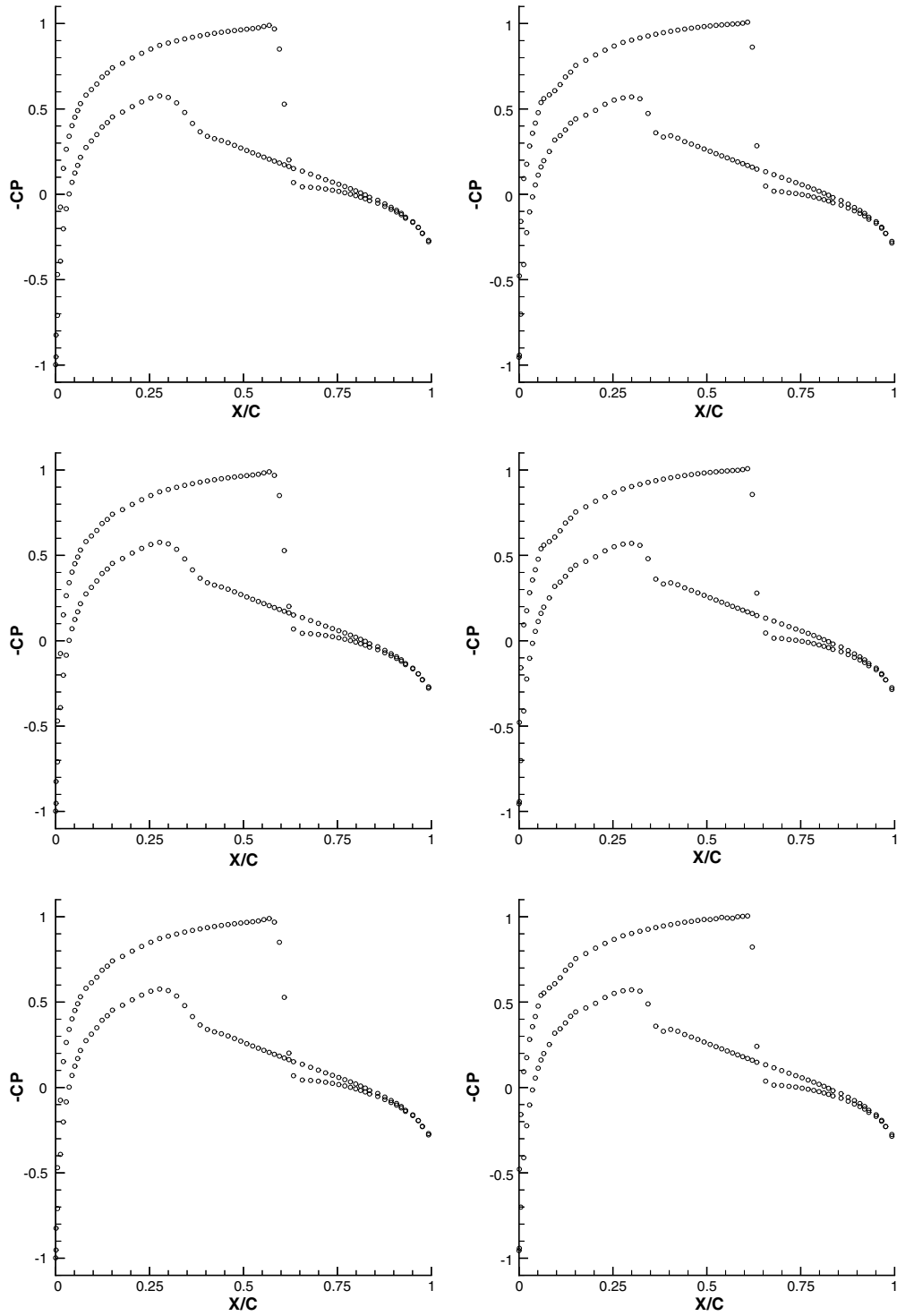


Fig. 3.14. NACA0012 airfoil. $M_\infty = 0.8$, angle of attack $\alpha = 1.25^\circ$. Pressure distribution. RKDG with the WENO limiter. Left: second order ($k = 1$); right: third order ($k = 2$). Top: the TVB constant $M = 1$; middle: $M = 10$; bottom: $M = 100$.

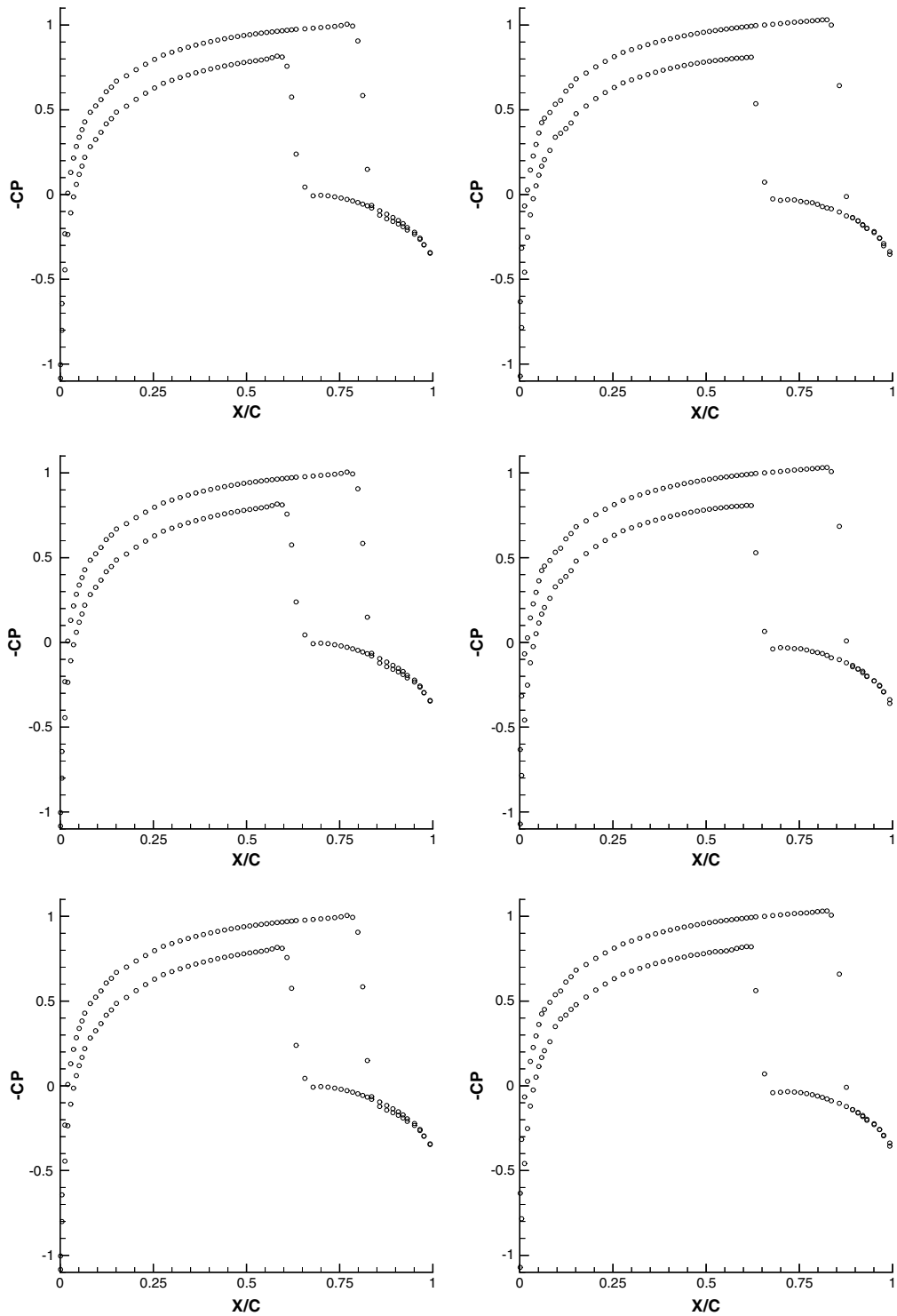


Fig. 3.15. NACA0012 airfoil. $M_\infty = 0.85$, angle of attack $\alpha = 1^\circ$. Pressure distribution. RKDG with the WENO limiter. Left: second order ($k = 1$); right: third order ($k = 2$). Top: the TVB constant $M = 1$; middle: $M = 10$; bottom: $M = 100$.

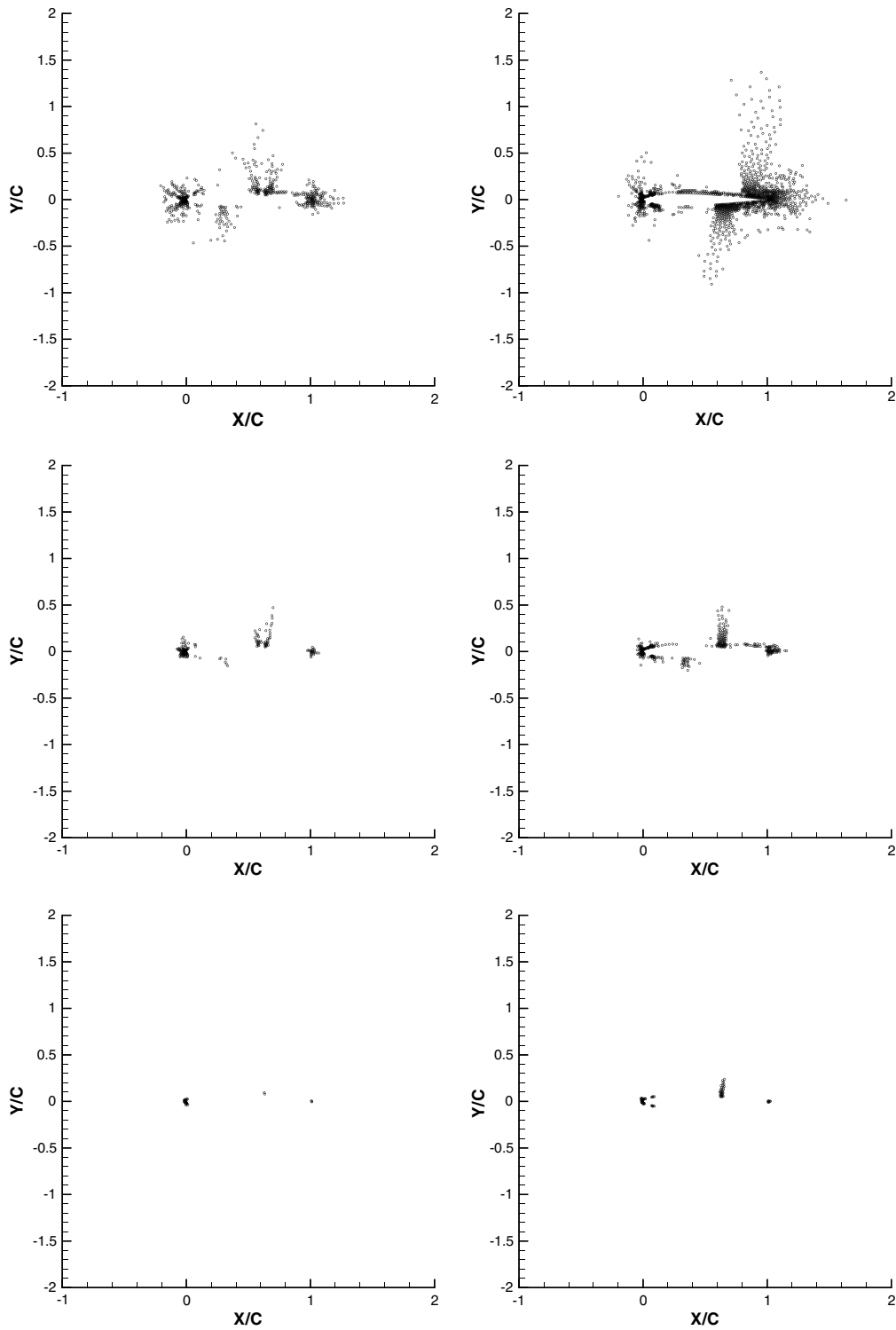


Fig. 3.16. NACA0012 airfoil. $M_\infty = 0.8$, angle of attack $\alpha = 1.25^\circ$. Troubled cells. Circles denote triangles which are identified as “troubled cells” subject to the WENO limiting, RKDG with WENO limiter. Left: second order ($k = 1$); right: third order ($k = 2$). Top: the TVB constant $M = 1$; middle: $M = 10$; bottom: $M = 100$.

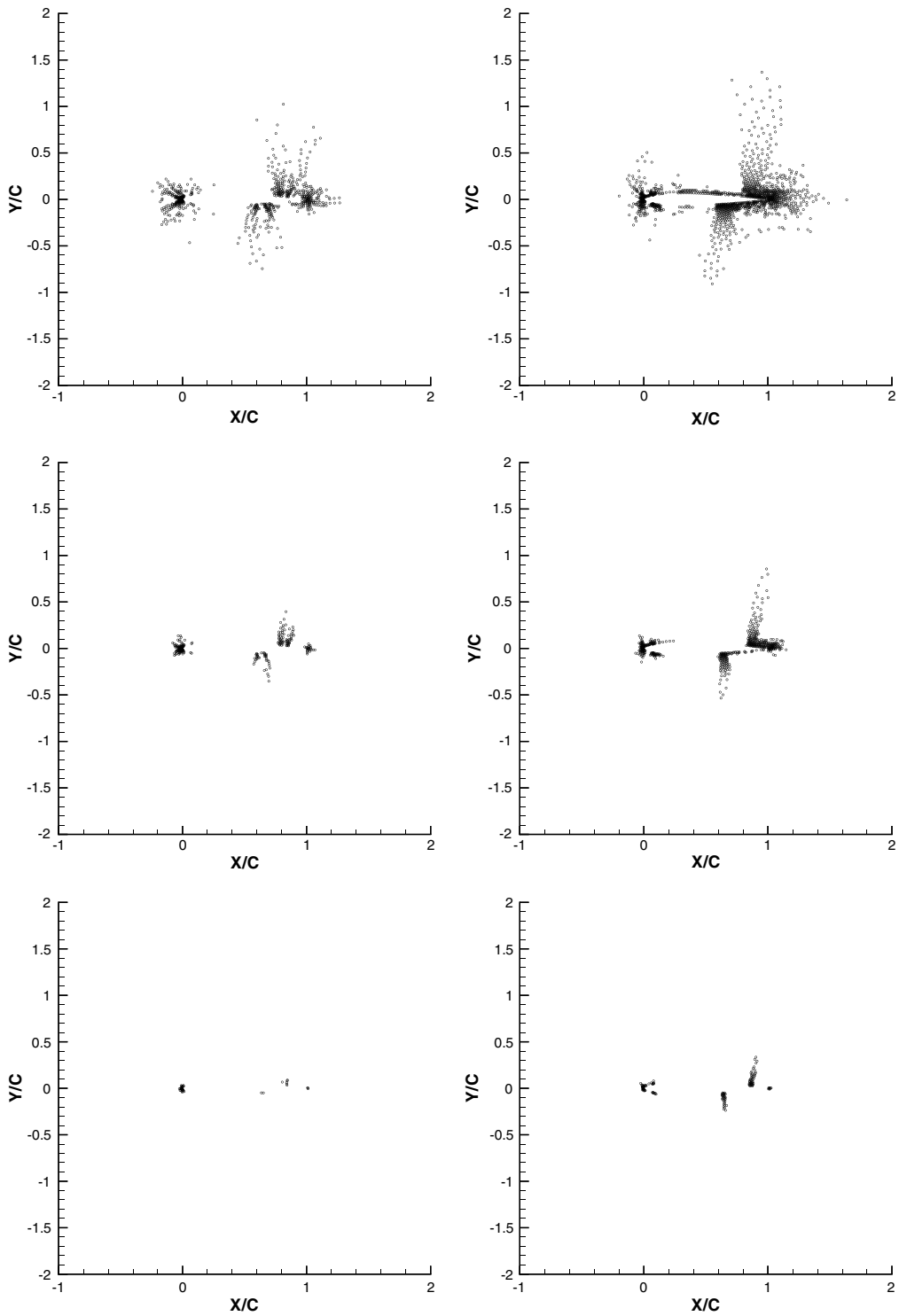


Fig. 3.17. NACA0012 airfoil. $M_\infty = 0.85$, angle of attack $\alpha = 1^\circ$. Troubled cells. Circles denote triangles which are identified as “troubled cells” subject to the WENO limiting. RKDG with WENO limiter. Left: second order ($k = 1$); right: third order ($k = 2$). Top: the TVB constant $M = 1$; middle: $M = 10$; bottom: $M = 100$.

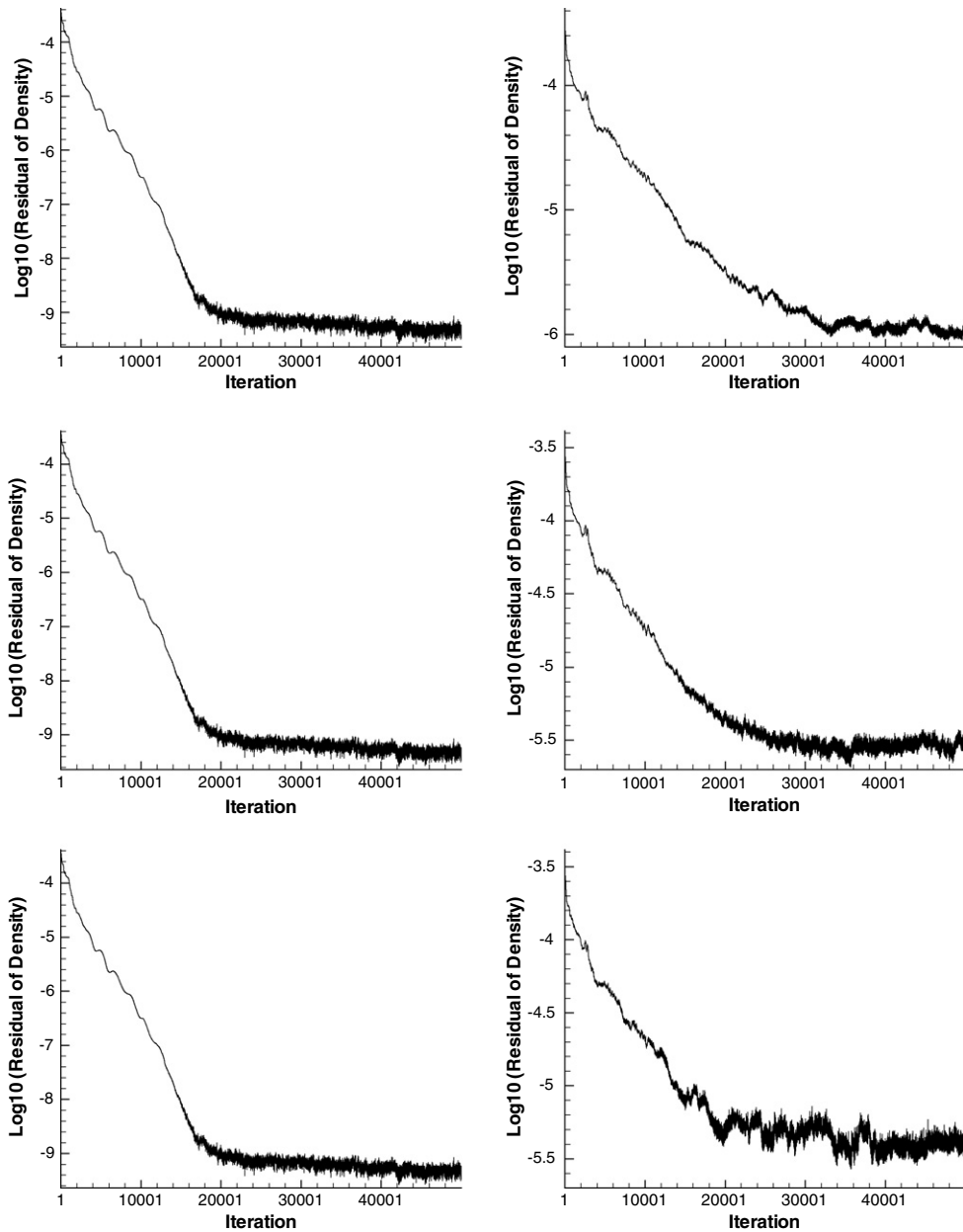


Fig. 3.18. NACA0012 airfoil. $M_\infty = 0.8$, angle of attack $\alpha = 1.25^\circ$. Reduction of density residual as a function of the number of iterations. RKDG with WENO limiter. Left: second order ($k = 1$); right: third order ($k = 2$). Top: the TVB constant $M = 1$; middle: $M = 10$; bottom: $M = 100$.

Acknowledgments

Jun Zhu was partially supported by the European project ADIGMA on the development of innovative solution algorithms for aerodynamic simulations, and by NSFC grant 10671091. Jianxian Qiu was partially supported by the European project ADIGMA on the development of innovative solution algorithms for aerodynamic simulations, NSFC Grant 10671091, SRF for ROCS, SEM and JSNSF BK2006511. Chi-Wang Shu was partially supported by NSF Grants AST-0506734 and DMS-0510345. Michael Dumbser was funded by the DFG Forschungsstipendium DU 1107/1-1.

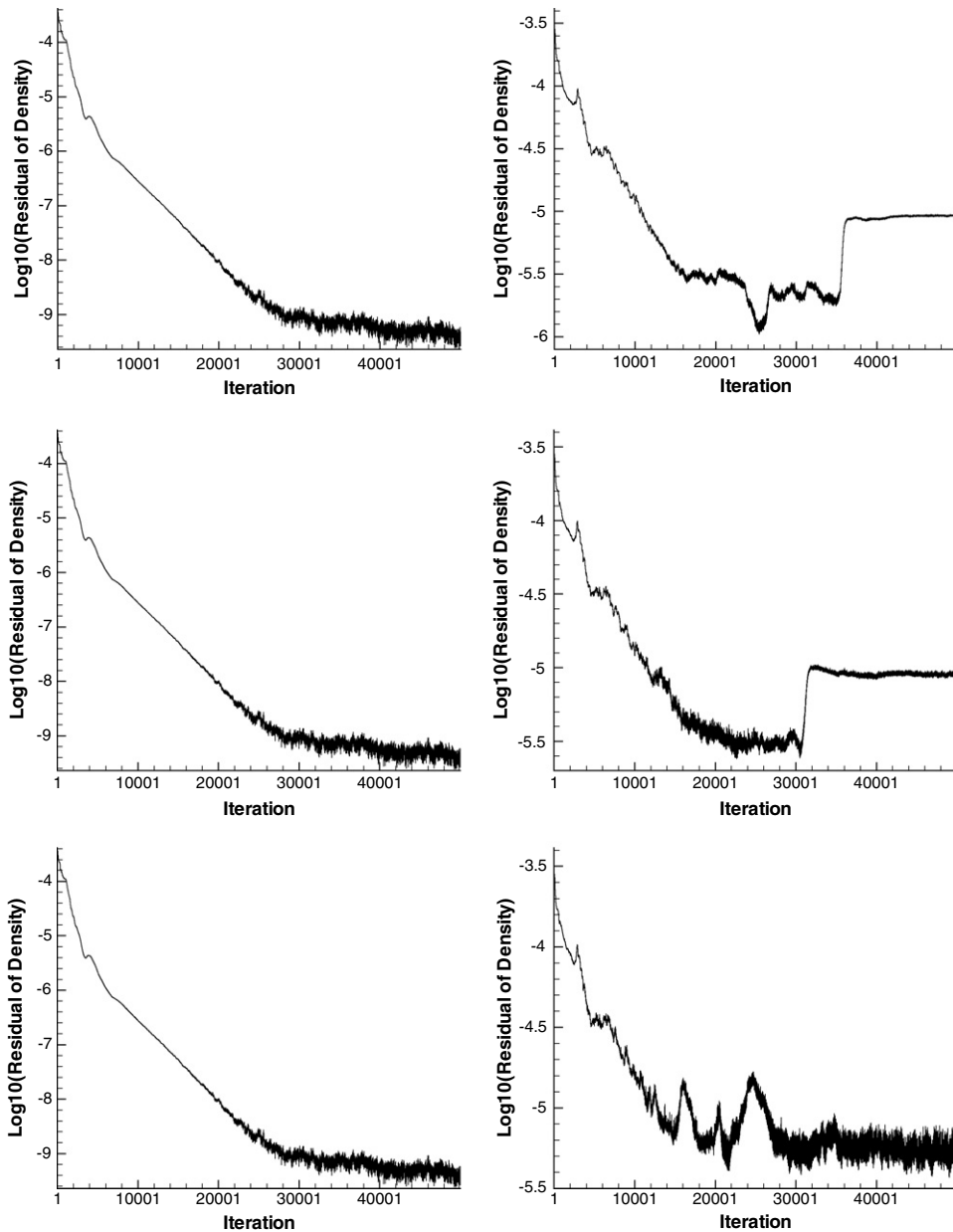


Fig. 3.19. NACA0012 airfoil. $M_\infty = 0.85$, angle of attack $\alpha = 1^\circ$. Reduction of density residual as a function of the number of iterations. RKDG with WENO limiter. Left: second order ($k = 1$); right: third order ($k = 2$). Top: the TVB constant $M = 1$; middle: $M = 10$; bottom: $M = 100$.

References

- [1] R. Biswas, K.D. Devine, J. Flaherty, Parallel, adaptive finite element methods for conservation laws, *Applied Numerical Mathematics* 14 (1994) 255–283.
- [2] A. Burbeau, P. Sagaut, C.H. Bruneau, A problem-independent limiter for high-order Runge–Kutta discontinuous Galerkin methods, *Journal of Computational Physics* 169 (2001) 111–150.
- [3] B. Cockburn, S. Hou, C.-W. Shu, The Runge–Kutta local projection discontinuous Galerkin finite element method for conservation laws IV: the multidimensional case, *Mathematics of Computation* 54 (1990) 545–581.

- [4] B. Cockburn, S.-Y. Lin, C.-W. Shu, TVB Runge–Kutta local projection discontinuous Galerkin finite element method for conservation laws III: one dimensional systems, *Journal of Computational Physics* 84 (1989) 90–113.
- [5] B. Cockburn, C.-W. Shu, TVB Runge–Kutta local projection discontinuous Galerkin finite element method for conservation laws II: general framework, *Mathematics of Computation* 52 (1989) 411–435.
- [6] B. Cockburn, C.-W. Shu, The Runge–Kutta local projection P1-discontinuous Galerkin finite element method for scalar conservation laws, *Mathematical Modelling and Numerical Analysis (M²AN)* 25 (1991) 337–361.
- [7] B. Cockburn, C.-W. Shu, The Runge–Kutta discontinuous Galerkin method for conservation laws V: multidimensional systems, *Journal of Computational Physics* 141 (1998) 199–224.
- [8] B. Cockburn, C.-W. Shu, Runge–Kutta discontinuous Galerkin method for convection-dominated problems, *Journal of Scientific Computing* 16 (2001) 173–261.
- [9] M. Dumbser, M. Käser, Arbitrary high order non-oscillatory Finite Volume schemes on unstructured meshes for linear hyperbolic systems, *Journal of Computational Physics* 221 (2007) 693–723.
- [10] M. Dumbser, M. Käser, V.A. Titarev, E.F. Toro, Quadrature-free non-oscillatory finite volume schemes on unstructured meshes for nonlinear hyperbolic systems, *Journal of Computational Physics* 226 (2007) 204–243.
- [11] O. Friedrichs, Weighted essentially non-oscillatory schemes for the interpolation of mean values on unstructured grids, *Journal of Computational Physics* 144 (1998) 194–212.
- [12] A. Harten, B. Engquist, S. Osher, S. Chakravathy, Uniformly high order accurate essentially non-oscillatory schemes, III, *Journal of Computational Physics* 71 (1987) 231–303.
- [13] C. Hu, C.-W. Shu, Weighted essentially non-oscillatory schemes on triangular meshes, *Journal of Computational Physics* 150 (1999) 97–127.
- [14] G. Jiang, C.-W. Shu, Efficient implementation of weighted ENO schemes, *Journal of Computational Physics* 126 (1996) 202–228.
- [15] D. Levy, G. Puppo, G. Russo, Central WENO schemes for hyperbolic systems of conservation laws, *Mathematical Modelling and Numerical Analysis (M²AN)* 33 (1999) 547–571.
- [16] X. Liu, S. Osher, T. Chan, Weighted essentially non-oscillatory schemes, *Journal of Computational Physics* 115 (1994) 200–212.
- [17] H. Luo, J.D. Baum, R. Lohner, A Hermite WENO-based limiter for discontinuous Galerkin method on unstructured grids, *Journal of Computational Physics* 225 (2007) 686–713.
- [18] J. Qiu, C.-W. Shu, On the construction, comparison, and local characteristic decomposition for high order central WENO schemes, *Journal of Computational Physics* 183 (2002) 187–209.
- [19] J. Qiu, C.-W. Shu, Hermite WENO schemes and their application as limiters for Runge–Kutta discontinuous Galerkin method: one dimensional case, *Journal of Computational Physics* 193 (2004) 115–135.
- [20] J. Qiu, C.-W. Shu, Runge–Kutta discontinuous Galerkin method using WENO limiters, *SIAM Journal on Scientific Computing* 26 (2005) 907–929.
- [21] J. Qiu, C.-W. Shu, Hermite WENO schemes and their application as limiters for Runge–Kutta discontinuous Galerkin method II: two-dimensional case, *Computers and Fluids* 34 (2005) 642–663.
- [22] W.H. Reed, T.R. Hill, Triangular mesh methods for neutron transport equation, Tech. Report LA-UR-73-479, Los Alamos Scientific Laboratory, 1973.
- [23] J. Shi, C. Hu, C.-W. Shu, A technique of treating negative weights in WENO schemes, *Journal of Computational Physics* 175 (2002) 108–127.
- [24] C.-W. Shu, TVB uniformly high-order schemes for conservation laws, *Mathematics of Computation* 49 (1987) 105–121.
- [25] C.-W. Shu, S. Osher, Efficient implementation of essentially non-oscillatory shock-capturing schemes, *Journal of Computational Physics* 77 (1988) 439–471.
- [26] C.-W. Shu, S. Osher, Efficient implementation of essentially non-oscillatory shock capturing schemes II, *Journal of Computational Physics* 83 (1989) 32–78.
- [27] P. Woodward, P. Colella, The numerical simulation of two-dimensional fluid flow with strong shocks, *Journal of Computational Physics* 54 (1984) 115–173.
- [28] Y.-T. Zhang, C.-W. Shu, Third order WENO scheme on three dimensional tetrahedral meshes, *Communications in Computational Physics* (submitted for publication).